

First Thermal IR Images of Neptune: Evidence for Southern Polar Heating and Methane Escape

Thérèse Encrenaz¹
 Glenn S. Orton²
 Cédric Leyrat²
 Richard C. Puetter³
 Andrew J. Friedson²
 Eric Pantin⁴

¹ Laboratoire d'Etudes Spatiales et d'Instrumentation pour l'Astrophysique (LESIA), Observatoire de Paris, Meudon, France

² Jet Propulsion Laboratory (JPL), California Institute of Technology, USA

³ Center for Astrophysics and Space Sciences (CASS), University of San Diego, California, USA

⁴ Service d'Astrophysique (SAp), Département d'Astrophysique, de Physique Nucléaire, de Physique des Particules et d'Instrumentation Associée (DAPNIA), Commissariat à l'Energie Atomique (CEA), Gif-sur-Yvette, France

Images of Neptune have been obtained in the thermal range, in filters between 8 and 19 μm , using the VISIR mid-infrared imaging spectrometer at the VLT-UT3 (Melipal). They allow, for the first time, mapping of atmospheric temperatures at different altitude levels, ranging from the tropopause to the stratosphere. It was found that the south pole of Neptune, at the level of the tropopause, appears to be warmer than the rest of the planet by 6 to 8 K. This southern polar warming can be explained by its constant solar illumination over the past 40 years, as the southern summer solstice occurred in July 2005. The other unexpected discovery is the evidence for a stratospheric hot spot located at 65–70°S which rotates with the planet at the atmospheric rotation rate of about 12 hours.

Neptune: a very active planet

In spite of its large heliocentric distance, Neptune is known to be dynamically very active. The first evidence came from Voyager 2 visible images at the time of the spacecraft's flyby in 1989 (Smith et al. 1989). Subsequent images and spectra taken in the near-infrared showed a strong variability of Neptune's cloud structure. In addition, high zonal winds have been

measured, and IRIS/Voyager infrared measurements have shown that the stratosphere is surprisingly warm. The active meteorology of Neptune is likely to be linked to its internal source of energy, which is 1.6 times the solar energy absorbed.

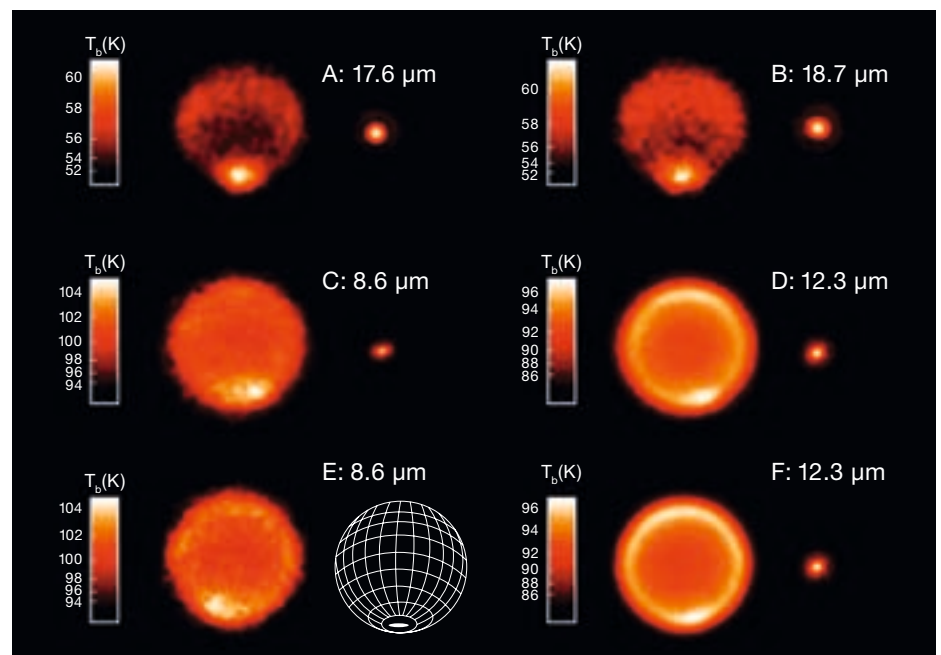
Other evidence for Neptune's high vertical circulation is the supersaturation of methane, which was discovered some twenty years ago from ground-based and space infrared spectroscopy. As for all the Giant Planets, the thermal profile of Neptune is characterised by a troposphere, where the temperature decreases with pressure, superimposed by a stratosphere where the temperature increases with the altitude. Between the two regions, the tropopause is the level of minimum temperature. Taking into account the low temperatures measured by Voyager at the tropopause of Neptune (typically 55 K at mid-latitudes), methane should be trapped at the tropopause and the CH_4 mixing ratio should be 3–10 \times

10^{-4} . In contrast, values several times higher were reported, which implied the existence of strong vertical motions; the mechanism of such circulation, however, was not understood.

Observations with VISIR

The mid-infrared camera/spectrometer VISIR, at the VLT-UT3 (Melipal) enabled us to map Neptune's atmospheric temperatures at all latitudes including the south pole, something Voyager had not been able to achieve during the spacecraft's flyby. The VISIR instrument (Lagage et al. 2004) operated in two modes, imaging and spectroscopy, between 7 and 25 μm . We selected different filters which allowed us to probe different levels of Neptune's troposphere and stratosphere. Observations were obtained on 1 and 2 September 2006. Two images of Neptune were obtained at 17.6 and 18.7 μm (see Figure 1). In this wavelength range, the spectrum of Neptune is sensitive to the collision-induced absorption (CIA) spectrum of hydrogen, due to $\text{H}_2\text{-H}_2$ and $\text{H}_2\text{-He}$ collisions, which is the major source of opacity. Because hydrogen is the major atmospheric constituent in Neptune's atmosphere, this measurement can be directly translated into an atmospheric temperature. At 18 μm , Neptune's radiation mostly comes

Figure 1: Thermal images of Neptune, with North at the top and the south pole visible at the bottom of each image. Images of nearby calibration stars (HD25025 for A, HD216032 for B, HD200914 for C, HD200514 for D and F) are also shown. Images C and E are separated by 6.83 hours in time; images D and F are separated by 2.25 hours.



from the tropopause, at a pressure about 100 mbars, where the temperature is minimum on all giant planets.

Other images were taken at 8.6 μm and 12.3 μm (Figure 1). At 8.6 μm the opacity is dominated by a CH_3D band (with some contribution from the wing of the strong CH_4 ν_4 band centred at 7.7 μm) and the radiation mostly comes from the stratosphere at 0.1 mbar. At 12.3 μm , the main absorber is C_2H_6 and the radiation also peaks at a level close to 0.1 bar. Ethane, like acetylene C_2H_2 and other hydrocarbons, is a photodissociation product of methane in the stratospheres of all giant planets. Two 8.6- μm images were taken, separated by 6.83 hours in time, and two 12.3- μm images were taken, separated by 2.25 hours (see Figure 1). Figure 2 shows the contribution functions at 8.6, 12.3, 17.6 and 18.7 μm . The two plots at 17.6 and 18.7 μm show a double structure; this is because they probe the tropopause and the lower stratosphere where the temperature increases sharply with altitude. The contribution function, which is the product of the opacity and the Planck function, thus exhibits two maxima.

Temperature increase at the south pole

Both images A and B of Figure 1 (at 17.6 and 18.7 μm respectively) show a strong maximum at the south pole of the planet. In addition, a local minimum appears at mid-southern latitudes and a weak increase is also visible in the equatorial region.

We processed the images using the ESO pipeline (Lagage et al. 2006) and we deconvolved them using the Pixon approach (Puetter and Yahil 1999). After deconvolution, it appeared that the southern bright spot exactly fits the position of the south pole (Figure 3). In order to retrieve the temperature at the tropopause as a function of latitude, we started from a mean thermal profile consistent with previous ground-based and Voyager measurements (Orton et al. 1992; Conrath et al. 1998) and we allowed for a translation by a few degrees to get the best fit. The result is shown in Figure 4, for both deconvolved images A and B. Voyager results (Conrath et al. 1998), ob-

tained between 20°N and 80°S by the IRIS infrared spectrometer, are also shown for comparison. Both images A and B lead to a strong increase of the temperature at the south pole, by about 10 K relative to 60°S latitude, and by about 7 K relative to the equator. The agreement with Voyager data is satisfactory at mid-latitudes, but the Voyager values tend to be weaker at 80°S; no information is available from Voyager at higher southern latitudes.

What can be the explanation of such a phenomenon? Most likely, the temperature increase at the south pole of Neptune results from its constant illumination over the past forty years. Neptune's sidereal period around the Sun is 164 years, and the last southern summer solstice occurred in July 2005. We can expect the opposite phenomenon in the future several decades, after the northern spring equinox, when the north pole of Neptune becomes illuminated. We also note that a similar effect was observed on Saturn (Orton and Yanamandra-Fisher 2005).

Methane escape in Neptune's stratosphere

The temperature excess at the south pole has an important consequence. If we consider the averaged temperature profile of Neptune, as derived from previous observations (Figure 4), methane, the most abundant minor atmospheric constituent (at the per cent level, far below hydrogen and helium), should be trapped at the tropopause in the form of ice. In the stratosphere, its mixing ratio should be constrained by the saturation low at the tropopause. Taking a temperature of 55 \pm 2 K at the tropopause, the mixing ratio should be 3–10 \times 10⁻⁴. In contrast, much higher values (0.75–1.5 \times 10⁻³) were measured by infrared spectroscopy, from the ground (Orton et al. 1992) or from the ISO Earth-orbiting satellite (Bézard et al. 1999). Recent measurements by Spitzer have also confirmed this result. It was then proposed that the atmosphere of Neptune had an active vertical circulation, able to transport the tropospheric methane from the troposphere up to stratospheric levels. However, as all these results were obtained on the integrated disc of Neptune, no information could be

obtained on its precise mechanism.

The VISIR images allow us to find an explanation to the circulation process. At the south pole of Neptune, the temperature of 63 K allows a methane mixing ratio of 8 \times 10⁻³, i.e. about eight times higher than the average observed value. North of 60°S latitude, the CH_4 mixing ratio allowed by the mean temperature of 55 \pm 2 K is, as mentioned above, about two times lower than the mean observed value. It is quite plausible that the active circulation of Neptune transports stratospheric methane from the south pole toward mid-latitudes where it condenses again as it falls down toward the tropopause.

If this explanation is correct, we would expect to find enhanced emissions of acetylene (C_2H_2) and ethane (C_2H_6) around the south pole. These molecules have strong infrared spectral signatures, at 13.7 μm and 12.5 μm respectively, which have been observed at high resolution from the ground and from ISO over the averaged disc of Neptune (Bézard et al. 2000). High-resolution imaging spectroscopy should be able to detect an asymmetry in their latitudinal profiles.

A hot spot in the stratosphere

Another surprise came from the VISIR images. The two 8.6- μm images C and E (Figure 1) clearly show a hot spot at about 65–70°S latitude, which appears at two different positions relative to the central meridian. Assuming it is the same spot on both images, we can calculate its rotation period. Both images are separated by 6.83 hours in time. After deconvolution, the inferred rotation period at 65–70°S latitude is about 12.4 \pm 1.3 hours. We note that this value is slightly different from the value of 13.8 hours quoted in the article where the present results are reported (Orton et al. 2007). The difference comes from a more precise treatment of the images. We believe that our last value is more reliable. It is, by the way, fully consistent with the value of 12.5 hours reported by Limaye and Sromovsky (1991) from cloud motion measurements at this latitude. It is definitely incompatible with the magnetic rotation period of 16.1 hours (Zarka et al.

1995), which implies that the observed spot is not associated with auroral processes. This interpretation would have been most unlikely anyway, as the magnetic pole of Neptune is tilted by 47° with respect to its rotational axis; thus any feature connected to the magnetic field would be expected to appear, 6.8 hours later, at a different latitude.

The two 12.3- μm images D and F (Figure 1), separated by 2.25 hours in time, also show a hot spot at about the same position, in latitude and longitude, as the 8.6- μm images. They also show a significant limb-brightening all around the planet, which probably results from a sharp increase of the temperature in the stratospheric region probed by the C_2H_6 emission (Figure 2).

What could be the origin of the observed hot spot? It is the signature of a localised atmospheric heating, at a pressure level of about 0.1 mbar. We could think of a cometary or asteroidal impact, comparable in nature with the SL9-Jupiter collision, but weaker. Since the discovery of oxygen-bearing compounds (CO , CO_2 , H_2O) in Neptune's stratosphere, it has been suggested that the oxygen flux might originate from cometary impacts (Lellouch et al. 2005). However, there is no evidence from any other observation of Neptune, in the visible, infrared or millimetre range, that a cometary impact took place over the past years.

Another more plausible explanation might be that the observed feature has a dynamical origin. The tropopause region is known to exhibit a strong variability of the cloud structure, especially near the pole. The warm polar temperature at the tropopause could be the tracer of a polar vortex which could extend into the stratosphere and generate localised stratospheric enhancements; however this assumption remains to be validated.

How to proceed further?

The next step of this work will consist in measuring the stratospheric mixing ratio of methane as a function of latitude. In the emission bands of hydrocarbons, at 8.6 and 12.3 μm , the outgoing flux depends upon two parameters: the mixing

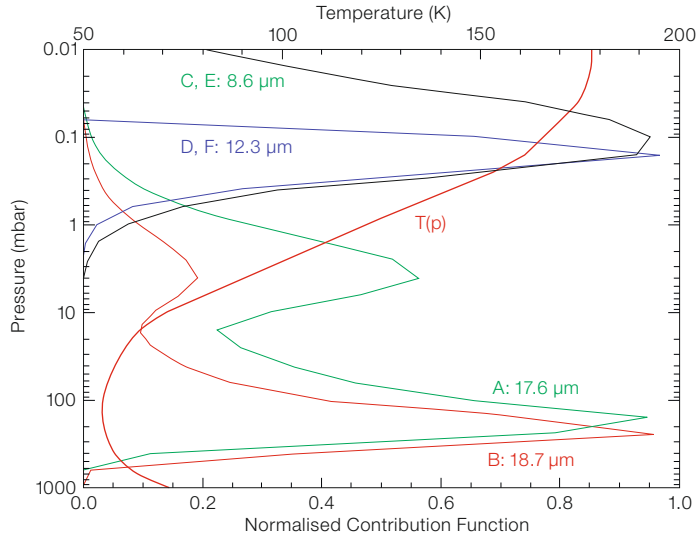


Figure 2: Contribution functions showing the origin of the outgoing radiance in the four filters used at 8.6, 12.3, 17.6 and 18.7 μm . For the 17.6 and 18.7- μm filters, the weighting function peaks just below the tropopause, and the upper maximum is the result of the sharp temperature increase in the lower stratosphere.

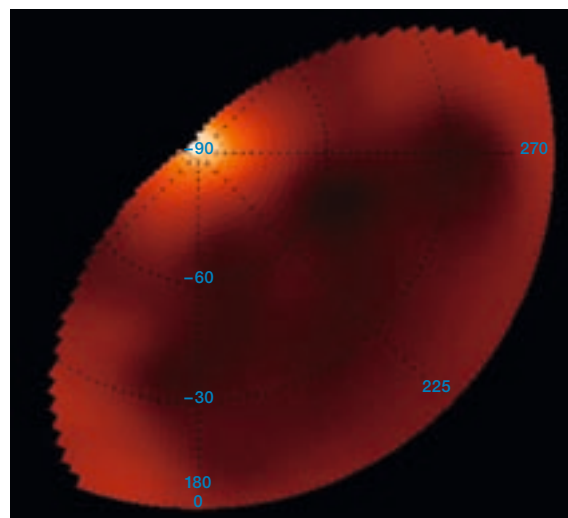


Figure 3: Polar projection of the de-convolved 17.6- μm image of Neptune. It can be seen that the centre of the hot spot exactly coincides with the south pole.

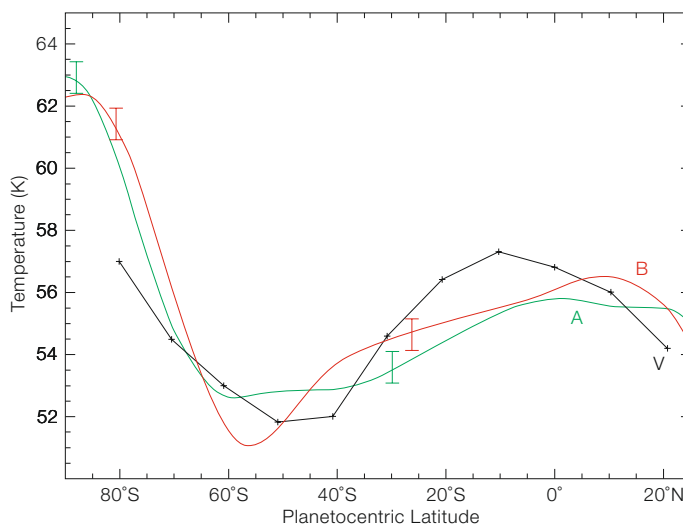


Figure 4: Latitudinal variations of the zonal mean temperature at the tropopause level (at a pressure level of 100 mbar). The green curve corresponds to Image A (in Figure 1); the red curve to Image B; and the black curve to Voyager results (Conrath et al. 1998).

ratio of the hydrocarbon and the temperature. It is thus necessary to determine independently the stratospheric temperature as a function of latitude. This can be done by high-resolution imaging spectroscopy of the S(1) quadrupole line of H_2 at $17.1 \mu\text{m}$. Such a measurement was achieved on 3 September 2006, using the spectroscopic mode of VISIR, and is presently under reduction and analysis. Another important measurement would be high-resolution imaging spectroscopy of the most intense hydrocarbon emissions in specific individual lines (C_2H_2 at $13.7 \mu\text{m}$, C_2H_6 around $12.5 \mu\text{m}$). These emissions, much stronger than CH_4 at $7.7 \mu\text{m}$, are very good tracers of stratospheric methane and can be used, through photochemical models, to infer the CH_4 mixing ratio.

Why are Uranus and Neptune so different?

In conclusion, it is interesting to note how different Uranus and Neptune are. In

spite of their common status as “icy giants”, and their similarities in global atmospheric composition and tropospheric temperature structure, they differ from each other in many ways. First Neptune, as mentioned above, has an internal source of energy, while none has been detected on Uranus. Second, Neptune has a very efficient dynamical circulation, while Uranus has no sign of one. Third, in contrast with Uranus, CO and HCN are very abundant in Neptune’s stratosphere. To account for all these differences, it has been suggested that both planets might have different internal structures. In Neptune, the heat (originating from the cooling of the planet since its formation) is transported from the interior by convection. Uranus, closer to the Sun, receives more solar flux than Neptune, which already hampers the escape of internal heat. In addition, the interior of Uranus might have a different stratification, so that convection might be inhibited, which would prevent the upward transport of internal energy. This hypothesis however remains to be tested.

Acknowledgements

We acknowledge the great help of the ESO staff at the VLT for making these observations possible. We thank the SAP-DAPNIA staff who built the VISIR instrument. We are grateful to K. Baines, H. Hammel, A. Mainzer, V. Meadows, K. Rages and L. Sromovsky for useful comments and support. This research was supported by JPL, NASA, Observatoire de Paris, CNRS and CEA.

References

- Bézar B. et al. 1999, ESA SP-427, 153
 Conrath B. J. et al. 1998, Icarus 135, 501
 Lagage P. O. et al. 2004, The Messenger 117, 12
 Lagage P. O. 2006, Proc. SPIE 6269, 626913
 Lellouch E. et al. 2005, A&A 430, L37
 Limaye S. S. and Sromovsky L. A. 1991, Nature 354, 380
 Orton G. S. et al. 1992, Icarus 100, 541
 Orton G. S. et al. 2007, A&A 473, L5
 Orton G. S. and Yanamandra-Fisher P. 2005, Science 307, 696
 Puetter R. C. and Yahil A. 1999, ASPCS 172, 307
 Sromovsky L. A. et al. 1993, Icarus 105, 140
 Zarka P. et al. 1995, in “Neptune and Titan”, University of Arizona Press, 341

Photo: H. H. Hoyer, ESO



An aerial view of the ESO Headquarters in Garching taken in summer 2007. For the required expansion of the ESO Headquarters building, an extension is being planned, for which an architect competition is in progress. The new building will be sited in the ploughed field to the south of the existing complex.

Polarimetry of Solar System Gaseous Planets

Franco Joos, Hans Martin Schmid
(Institute of Astronomy, ETH Zurich,
Switzerland)

With the ESO 3.6-m telescope and EFOSC2 we have observed Solar System planets to investigate limb polarisation in detail. Our observations were successful and we can report the detection of limb polarisation in Uranus and Neptune. In addition spatially resolved long-slit spectropolarimetry was obtained for the first time for all the gaseous planets. The observations reveal a decrease of limb polarisation with increasing wavelength and an enhanced polarisation in the methane bands against the adjacent continuum. We describe our measurements and also discuss the diagnostic potential of such data for the investigation of the atmospheric structure of giant planets and the properties of their scattering particles.

Science motivation

Light reflected from planets is polarised. This basic property provides the opportunity to investigate planetary atmospheres by means of polarimetry. Many previous studies of Solar System planets demonstrate that polarimetry is a very powerful tool for the investigation of the atmospheric structure and the characterisation of the scattering particles. Well-known examples are the studies of the polarisation of Venus (e.g. Dollfus and Coffeen 1970), which permitted the determination of the droplet size and composition in the reflecting clouds. Other famous examples are the highly polarised poles of Jupiter which were first described by Lyot in 1929 (Lyot 1929). The polarisation at the poles is high because the radiation is reflected by Rayleigh scattering particles, while it is low at the equatorial limbs since there the light is reflected by clouds (see Figure 1). These examples illustrate well the diagnostic potential of polarimetry.

Polarimetry is also a very attractive technique for the search and investigation of extrasolar planets for three main reasons: firstly, the expected polarisation signal of the reflected light from a planet is high, on the order 5 to 50% for phase

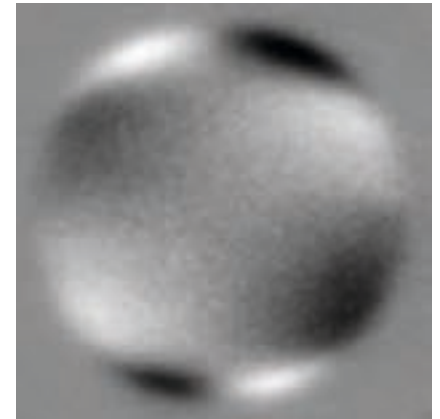
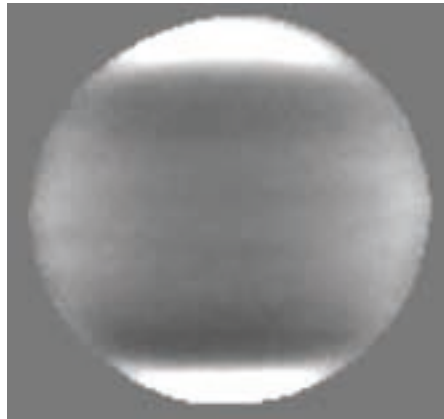


Figure 1: Imaging polarimetry of Jupiter. **Left:** the polarised Stokes Q flux, with white indicating positive (vertically) and black negative (horizontally) polarised light. **Right:** the polarised Stokes U flux (polarisation direction is rotated by 45° in a counter-clockwise direction compared with Q). Data taken with the Zurich imaging polarimeter system (ZIMPOL) at the McMath-Pierce solar telescope at Kitt Peak in a methane filter centred at 730 nm.

angles near 90° ; secondly, the reflected (= polarised) light can be distinguished from the unpolarised radiation from the central star; thirdly, the amount of polarisation provides information on the scattering particles and the atmospheric structure of the planet (see Schmid et al. 2006). Therefore, the future VLT planet finder instrument SPHERE (Spectro-Polarimetric High-contrast Exoplanet REsearch) will have a polarimetric mode in order to search for polarisation signals of extrasolar planets (Beuzit et al. 2006).

From the Earth all the giant planets are observed near zero phase angle (maximum phase angles are $\approx 11^\circ$ for Jupiter or $\approx 2^\circ$ for Neptune, for example) and essentially no polarisation is expected in integrated light. But if the planetary disc is resolved, then one can expect a limb polarisation, which arises due to a well-known second-order effect for reflecting atmospheres where Rayleigh type scattering processes are dominant (see e.g. van de Hulst 1980).

In order to understand the limb polarisation, one has to consider a back-scattering situation at the limb of a gas-rich planet, where there is locally a configuration of grazing incidence and grazing emergence for the incoming and the back-scattered photons, respectively.

Light reflected after one scattering is unpolarised, because the scattering angle is 180° . Photons undergoing two scatterings travel, after the first scattering, predominantly parallel to the surface before being reflected towards the observer by the second scattering process. The reason is that photons travelling outwards from the planet will mostly escape without a second scattering, while photons travelling inward have a low probability of being reflected towards the observer after the second scattering, but a high probability to be absorbed or to undergo multiple scatterings. Since the polarisation angle induced by a single dipole-type scattering process, like Rayleigh scattering, is perpendicular to the propagation direction of the incoming photon (which in this case is parallel to the limb), polarisation perpendicular to the limb is produced.

Limb polarisation of the giant planets has up to now hardly been investigated. Although there exist several studies based on filter polarimetry for Jupiter, and a few for Saturn, we have found no previous polarimetric observations which resolved the limb of Uranus and Neptune, nor disc-resolved spectropolarimetric measurements indicating limb polarisation. For this reason we proposed such observations with EFOSC2 at the ESO 3.6-m telescope.

Polarimetry with EFOSC2

The EFOSC2 instrument is a multi-mode Cassegrain imager and grism spectrograph which can be equipped with a Wollaston prism and a rotatable superachromatic half-wave plate for linear im-

aging polarimetry and spectropolarimetry. For linear polarimetry one measures the Stokes parameters Q and U , which are the differential intensity signals between two orthogonal linear polarisation directions according to $Q = I_0 - I_{90}$ and $U = I_{45} - I_{135}$ (where 0, 90, ... signify the polarisation direction on the sky). In EFOSC2 a Wollaston prism splits the light into the I_{\perp} and I_{\parallel} polarisation directions (relative to the orientation of the prism). The two images, called the ordinary and the extraordinary beams, are separated on the CCD by 10" or 20", respectively (see Figure 2). The two beams from the Wollaston do not overlap thanks to a special aperture mask in the focal plane with a series of open stripes (or slitlets for spectropolarimetry), whose width and separation correspond to the image separation introduced by the Wollaston beam splitter. Combining the polarimetric components with normal EFOSC2 filters or grisms then yields imaging polarimetry or spectropolarimetry, respectively (Figure 2).

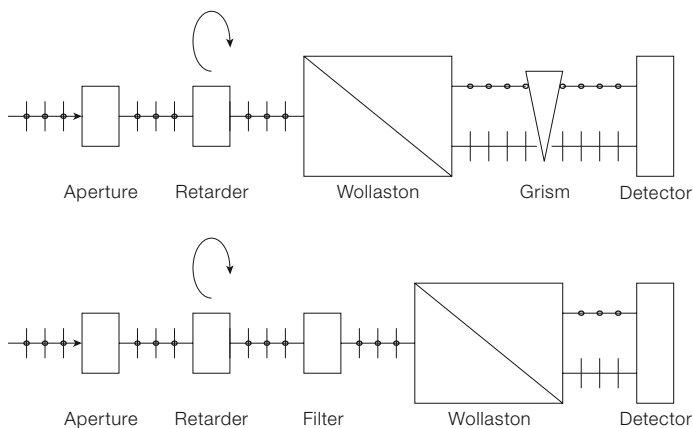


Figure 2: Schematic concept for spectropolarimetry (upper) and imaging polarimetry (lower).

Imaging polarimetry	Spectropolarimetry
Wollaston 10" stripe mask	Spectropolarimetric 20" slitlets
Half-wave plate	Half-wave plate
Broad- and narrowband filters	Wollaston prism 20"
Wollaston prism 10"	Grism ESO#5
CCD	CCD

Table 1: Set-ups for EFOSC2 imaging polarimetry and spectropolarimetry.

It is important for a high polarimetric precision that the two polarisation directions I_{\perp} and I_{\parallel} are measured simultaneously in order to avoid errors due to atmospheric seeing and transmission variations. Rotating the half-wave plate between two exposures, e.g. from 0° to 45° for Stokes Q , allows the two polarisation images to be swapped on the detector, so that differential effects in the two Wollaston beams cancel out in the polarisation signal (including the individual pixel efficiencies of the CCD). Thus, two frames taken with different retarder plate orientations yield one normalised Stokes parameter: Q/I with the half-wave plate orientations 0° and 45°; and U/I with the orientations 22.5° and 67.5° (cf. Tinbergen 1996).

The instrumental set-up for imaging polarimetry and spectropolarimetry for our planet observations is summarised in Table 1.

Figures 3 and 4 show examples of the raw frames for Uranus, taken in imaging polarimetry mode and spectropolarimetric mode, respectively. In imaging mode the ordinary and the extraordinary beams are separated by 10" in spectropolarimetric mode the separation is 20". The 20" long slit was oriented North-South over the disc of Uranus, approxi-

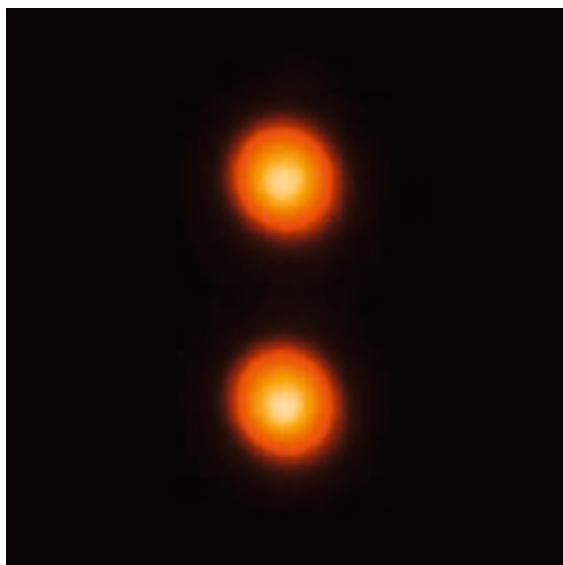


Figure 3: Raw data for an exposure of Uranus in imaging polarimetry mode. The ordinary and the extraordinary images are separated by 10". The two images are not perfectly round because Uranus showed a bright south pole and darker northern latitudes.



Figure 4: Raw data for an exposure of Uranus in spectropolarimetric mode. The deep methane absorption bands at longer wavelengths are clearly visible to the right.

mately along the planetary equator. This configuration yields long-slit spectropolarimetry, providing a centre to limb profile in intensity and polarisation for each wavelength covered by the grism.

EFOSC2 at the 3.6-m telescope is an ideal polarimetric instrument because it is attached to the Cassegrain focus and there are no strongly inclined optical components in the beam. The whole optical set-up is rotationally symmetric, so that the instrumental polarisation from the telescope and the instrument are essentially zero, at least near the optical axis. One problem of our observations was that the surface brightness of Jupiter and Saturn was too high for imaging polarimetry, even in narrowband filters. For this reason we inserted, together with some narrowband filters, an opaque mask near the pupil of EFOSC2. The mask was a self-made black plate with 28 small holes which blocked about 99% of the telescope light.

Imaging polarimetry of Uranus and Neptune

During two nights in visitor mode we were fortunate to often have subarcsec seeing conditions at the 3.6-m telescope. This allowed us to well resolve the discs of Uranus (diameter 3.5") and Neptune (2.2") and to detect the limb polarisation. The measured normalised polarisation was in the range 0.5 to 1.5% for both planets. Observations with *R* (644 nm), *i* (803 nm) and *z* (890 nm) band filters were taken for these two targets. The resulting *i*-band polarimetry is shown in Figures 5 and 6. The position of the limb, the equator and the south pole are indicated.

The Stokes *Q* and *U* images for Uranus both show a very characteristic quadrant pattern. $Q = I_0 - I_{90}$ is positive (white in the figures) or vertical at the equatorial limbs, negative (black in the figures) or horizontal at the polar limbs, and essentially zero in the centre of the planetary disc. For *U* the same pattern is apparent but rotated by 45°. Neptune shows qualitatively the same pattern. In order to obtain these *Q* and *U* maps one has to carefully align the images from the ordinary and extraordinary beam. The precision has to be better than a tenth of a

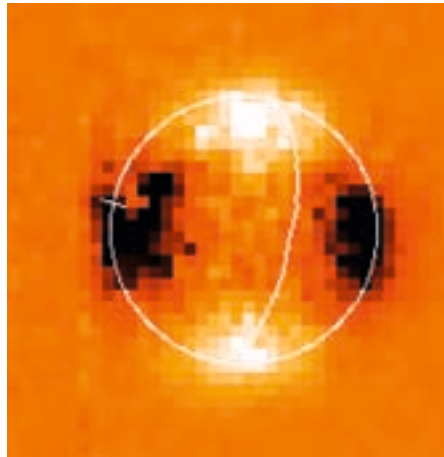


Figure 5 (above): Imaging polarimetry of Uranus in *i*-band; white corresponds to positive and black to negative polarisation. The limb is indicated by the circle, the equator by an arc and the south pole by the tick mark. **Left:** the polarised flux in the *Q*-direction with positive vertical and negative horizontal. **Right:** the polarised flux in the *U*-direction. The polarisation pattern is rotated by 45° in a counter-clockwise direction.

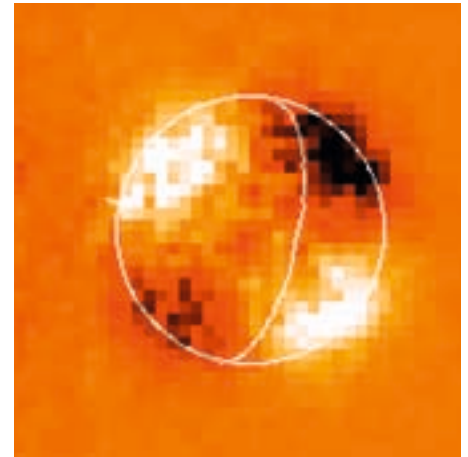
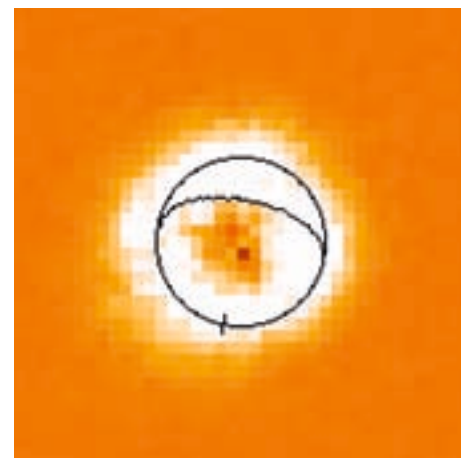
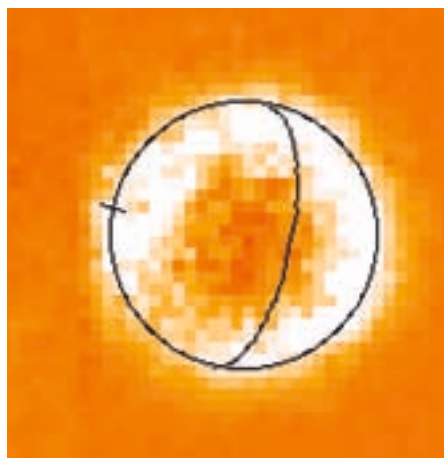


Figure 6 (below): Radial polarisation of Uranus and Neptune constructed from the *Q* and *U* images. White denotes radial polarisation and black would denote tangential polarisation, with orange as intermediate values. **Left:** Uranus in the *i*-band. **Right:** Neptune in the *R*-band.



pixel (1 pixel = 0.157"). A misalignment of one image would create a spurious positive polarisation signal at one limb and at the same time a spurious negative signal at the opposite limb.

The observed *Q* and *U* images indicate that the polarisation is high at the limb and low in the disc centre. The position angle of polarisation is perpendicular to the limb everywhere. This pattern can be better illustrated with a transformation to radial Stokes parameters Q_r and U_r , which are defined relative to the radial direction on the planetary disc. Positive Q_r indicates a radial polarisation and neg-

ative Q_r , a tangential polarisation, while $\pm U_r$ are the polarisations at $\pm 45^\circ$ orientation relative to the radial direction. The resulting Q_r images for Uranus and Neptune are shown in Figure 6. In both cases the limb polarisation is clearly visible as a bright ring with positive Q_r polarisation. The U_r images are essentially zero as there is no polarisation with a tilted orientation relative to the limb. The figures also suggest that the polarisation has a constant strength along the entire limb. This situation is unlike Jupiter (see Figure 1) or Saturn where significant limb polarisation is only observed at the poles.

For a quantitative analysis we have to take into account that the seeing-limited spatial resolution of our observations causes a degradation and cancellation in the polarisation. Our imaging polarimetry reveals that the limb polarisation decreases for both planets from the *R*- to *i*- to *z*-bands. From the Q_r maps it is also possible to derive the disc-integrated limb polarisation, which is a good parameter for comparing observations with model calculations. Unfortunately, there exists a severe lack of model calculations for limb polarisation. For this reason we compared our results with analytic calculations for Rayleigh scattering atmospheres from the 1970's and earlier, going back to the classical work of Chandrasekhar in 1950. Consulting these simple models indicates that the Rayleigh scattering layers in Uranus and Neptune have an optical depth of about $\tau = 0.2$ in the *R*-band continuum and lower for longer wavelengths. This dependence is expected as the Rayleigh scattering cross section behaves like $\sigma \propto 1/\lambda^4$. The polarisation is therefore higher for short wavelengths.

Spectropolarimetry

During the same observing run we also performed long-slit spectropolarimetry of the four giant gaseous planets. The spectropolarimetric mask consisted of a series of 20" long by 0.5" wide slitlets, aligned along a line and separated by 20" (corresponding to the beam separation of the Wollaston used for spectropolarimetry). We chose the grism ESO#5 which covers the spectral region 530 to 930 nm, providing a spectral resolution of 1.3 nm for a 1" wide slit. In this wavelength range the giant planets show a rich spectrum of weak and strong methane absorption bands. For Jupiter and Uranus we present in Figure 7 the extracted intensity (arbitrary scale) and polarisation spectrum for the limb.

For the observation of Uranus, the slit was oriented along the celestial N-S direction, covering the entire equatorial region from limb to limb. The intensity and polarisation signal were then extracted and averaged from the N and S limb regions with their high polarisation. For Jupiter the slit was aligned along the central meridian covering the northern parts

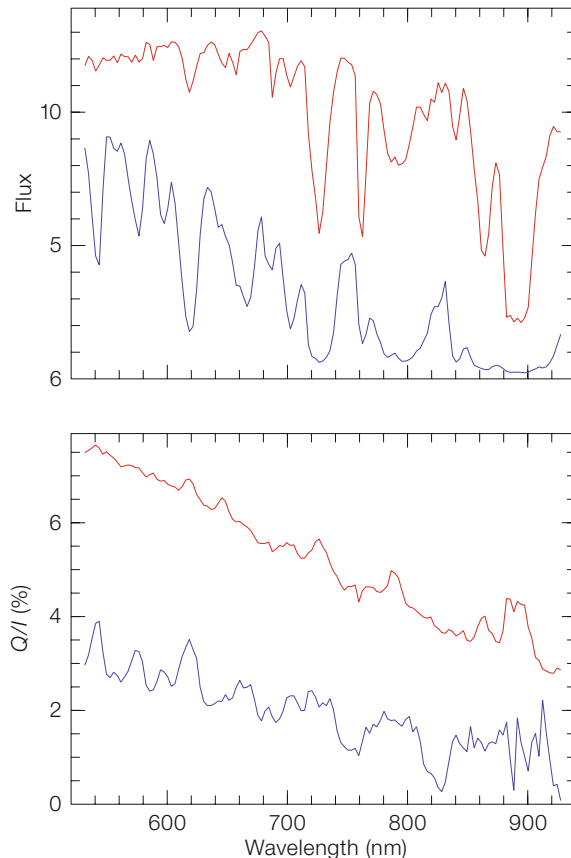


Figure 7: Spectropolarimetry for the limbs of Jupiter (red) and Uranus (blue). **Top:** flux in arbitrary units. **Bottom:** Stokes Q/I in per cent for both planets. For Uranus the polarisation signal is corrected for the degradation due to the seeing-limited resolution.

of the planet from about the centre to the limb. The diameter of Jupiter in the polar direction was 33.6". The Jupiter data in Figure 7 represent the high polarisation region at the northern limb. Further observations with different slit orientations were obtained for Jupiter and Uranus. Also Neptune and Saturn were observed in a similar way.

The data reduction turned out to be very demanding because the Wollaston introduces some dispersion perpendicular to the grism dispersion. This dispersion differs between the ordinary and extraordinary beams. Therefore, we had to align the two bent long-slit spectra to a precision of about a tenth of a pixel in the spatial direction in order to avoid spurious polarisation features due to misalignment. In the end we obtained two-dimensional long-slit spectropolarimetry providing for each wavelength disc profiles or centre-to-limb profiles for the intensity and polarisation.

First, we consider the spectropolarimetric signal of the limb. There are two general features which are present in all limb polarisation measurements of the giant planets (see Figure 7): the polarisation at the limb decreases to longer wavelengths; the polarisation is enhanced in the strong methane absorptions when compared to the adjacent higher flux regions. The overall decrease is due to the wavelength dependence of Rayleigh scattering, as already pointed out above. The enhanced polarisation in the methane bands can be explained with a two-layer model. An optically thin Rayleigh scattering layer producing the limb polarisation is located above a diffusely reflecting atmosphere or cloud layer, which reflects predominantly unpolarised light. Enhanced absorption in molecular bands efficiently reduces the unpolarised reflection of the lower layers resulting in a higher normalised polarisation for spectral regions with a low albedo.

There are significant quantitative differences in the polarisation properties of the

two planets. For example, the polarisation is very high at the poles of Jupiter, reaching values up to 9% in the V-band and the maxima in the normalised polarisation spectrum are quite narrow, due to narrow methane absorption bands. For Uranus the limb polarisation is lower, and accordingly, the polarisation maxima associated with the broad absorption bands are broader. Nevertheless, the relative polarisation enhancements in the methane bands are much more pronounced in Uranus.

Our long-slit spectropolarimetry also provides the centre-to-limb profile for the intensity and polarisation for each wavelength covered by the spectrum. For example, for Uranus we see in the strong absorption bands that the enhanced limb polarisation correlates with a limb brightening of the reflected intensity (cf. Joos and Schmid 2007). Both limb brightening and limb polarisation probe the uppermost layers of the reflecting atmospheres. Long-slit spectropolarimetry seems to be an ideal tool to investigate the structure and particle properties for these layers.

Prospects

Our polarimetric observations of the giant planets with EFOSC2 at the 3.6-m telescope demonstrate that detailed obser-

vational studies of the limb polarisation effect are possible. We have shown that a rich palette of observational parameters can be deduced from such observations and they can be used to constrain the atmospheric structure and particle properties. Additional investigations, including the still-pending analysis of our Saturn data, will further clarify the diagnostic potential of limb polarisation. Currently, an important stumbling block is the lack of detailed model calculations of the limb polarisation for realistic planetary atmospheres. Although computer codes for such model calculations exist (e.g. Braak et al. 2002), they need to be run for simulations of Earth-bound limb polarisation measurements, as presented in this article. Without such calculations we can at present only extract qualitative properties from our observations. Model calculations could significantly improve this situation.

The comparison of our data with simple (analytic) models of Rayleigh scattering atmospheres indicates that the detected limb polarisation is compatible with expectations. In general, the limb polarisation is due to Rayleigh scattering particles. They are located high in the planetary atmosphere, above layers of diffusely reflecting gas or clouds. The limb polarisation is high if the Rayleigh scattering layer is optically thick or if the penetrating

radiation is strongly absorbed in deeper layers, e.g. by methane.

For Uranus and Neptune, for which no polarimetry at large phase angles exist from space missions, we can extrapolate from the limb polarisation and estimate the expected disc integrated polarisation for phase angles near 90 degrees. We find that the polarisation must be high ($\rho > 20\%$) in the R-band. Such estimates are of interest for the interpretation of future polarimetric detections of extrasolar planets with the SPHERE VLT Planet Finder.

Acknowledgements

We are indebted to the ESO La Silla SCIOPS and the 3.6-m telescope team who were most helpful with our very special instrumental requirements. We are particularly grateful to Olivier Hainaut, Ivo Saviane and Emilio Barrios Rojas.

References

- Beuzit J. L. et al. 2006, *The Messenger* 125, 29
- Braak C. J. et al. 2002, *Icarus* 157, 401
- Dollfus A. and Coffeen D. L. 1970, *A&A* 8, 251
- Joos F. and Schmid H. M. 2007, *A&A* 463, 1201
- Lyot B. 1929, *Ann. Observ. Meudon* 8
- Schempp W. V. and Smith W. H. 1984, *Icarus* 77, 228
- Schmid H. M. et al. 2006, *IAU Coll* 200, 165
- Tinbergen J. 1996, *Astronomical polarimetry*, Cambridge University Press, 100
- van de Hulst H. C. 1980, *Multiple light scattering 2*, Academic Press



In August 2007 the Uranus ring system was almost exactly edge-on to Earth, an event which only occurs every 42 years. The two images show the Uranus system in November 2002, with the rings well displayed, and in August 2007 when the rings were edge-on and no longer visible. The image of 2002 was taken with ISAAC on the VLT while the one of 2007 was taken with NACO and made use of adaptive optics, explaining the higher resolution. The NACO image is a false colour composite based on images taken at wavelengths of 1.2 and 1.6 microns. See ESO PR 37/07 for more details.